ACS OMEGA

http://pubs.acs.org/journal/acsodf

Article

Three-Dimensional Physical Similarity Simulation Experiments for a Transparent Shaft Coal Pocket Wall in Coal Mines

Yongping Wu, Mingyin Liu,* Panshi Xie, Hongwei Wang, and Bosheng Hu

Cite This: *ACS Omega* 2022, 7, 16442−16453

Read Online

ACCESS | Metrics & More | Article Recommendations

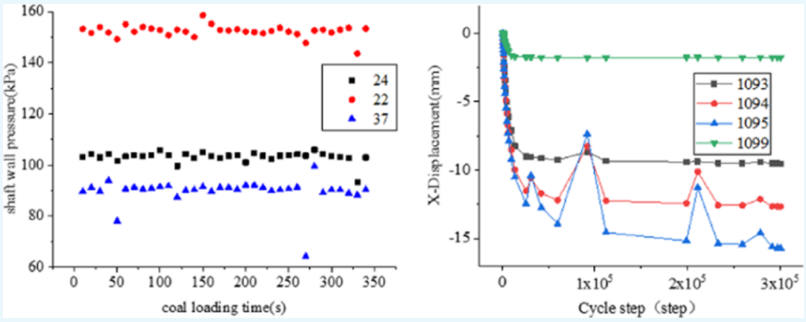

ABSTRACT: To explore the variations of the loading, deformation, and loss and to determine the mechanical state, loss characteristics, and stability for the shaft coal pocket wall in coal mines under a dynamic-static load, this paper innovatively attempts to conduct a three-dimensional physical similarity test of a transparent material shaft coal pocket, as well as the experiments of loading and unloading coal in the shaft coal pocket using different bulk storage materials 80 times. Then, the deformation, pressure, the surrounding rock, and the flow pattern of the silo wall were discussed considering the existence of the warehouse wall support. The characteristics of shaft wall deformation and surrounding rock stress cracks during the unloading were analyzed with the help from multiple integrated test systems such as strain gauges, pressure sensors, borehole peeps, and other comprehensive test systems. The results indicated that different dispersion particles have a significant impact on the strain of the shaft wall. When using the coal particles as storage materials, the overpressure coefficient of the shaft wall is up to 1.95 times higher than using dry sand particles. The particle size and internal friction angle of the bulk particles impact significantly on the deformation of the wall, where the cohesive force among the dispersed particles produced by the compaction effect has a certain influence on the side pressure of the silo wall. During the unloading process, coal particles were easier to obtain an arching phenomenon than dry sand particles. In addition, the number of bulk arching could be significantly reduced under the conditions of the warehouse wall support. The "weak rock stratum" in the surrounding rock plays a major role in controlling the deformation and failure development of the shaft wall. The three-dimensional physical simulation experiment of the transparent shaft wall truly reproduces the field engineering practice, and the physical simulation results are verified by numerical simulation analysis.

1. INTRODUCTION

As coal is the main non-renewable energy, it is necessary to investigate the underground bunker of coal fuel storage devices in coal mine production.[1−3] The underground shaft coal pocket serves as a throat project of the main transportation system of the coal mine, which has a great significance to ensure the safe production of the coal mine.[4−6] A three-dimensional physical similarity simulation experiment was an effective research method to investigate the loading, deformation, and loss of the shaft coal pocket wall in coal mining engineering practice. For the shaft coal pocket, the motion characteristics of the bulk material were complex for the bulk storage material in the bottom coal bunker.[7,8] The damage of the coal bunker wall at the bottom of the shaft could bring a series of problems such as a mine shutdown. Yang et al.[9] analyzed the localization mechanism of the sand particle system during the shear process through discrete element software. Wu et al. created the mechanical model of a three-dimensional structure of bulk particles of the bottom coal bunker and proposed the mechanism of unloading over-pressure on the silo wall.[10,11] The deformation law of buildings and surrounding rocks in underground engineering is helpful to better guide the field engineering practice.[12−14] Gentzis et

Received: January 21, 2022
Accepted: April 21, 2022
Published: May 4, 2022

https://doi.org/10.1021/acsomega.2c00450
ACS Omega 2022, 7, 16442−16453

al.[15] proposed that the wellbore stability was affected by the diameter of the hole, and a small diameter is conducive to wellbore stability. Xiao et al.[16] proposed that the settlement of coal bunker lags behind that of the surface. Xin et al.[17] analyzed the failure characteristics of gangue and proposed that there existed a straight-line rising section in the initial stage of the strain curve of loose gangue. Meng et al.[18] adopted the numerical analysis to clarify the soft rock stratum in the coal mine and examined the surrounding rock deformation. Other scholars also estimated the side pressure of the cylindrical shaft wall.[19−22] There still exist some pending issues, which need to be investigated such as the stability of the shaft coal pocket wall, bulk flow properties, and the induced change of mechanical behaviors of the contact surface between the surrounding rock and the shaft wall.[23−27] Nedderman and Léonard et al. studied about the bunker stress distribution.[28,29] Different coal particles have different properties due to their different components, so the impact is different. Akinyemi et al. based on vitrinite reflectance classified the coal samples from the Benue Trough sedimentary basin in Nigeria.[30] Hood[31] and Yalcin[32] et al. studied about the organic fraction of the coals; Guatame and Rincón analyzed the coal facies changes in the depositional conditions of the sequence in the Eastern Cordillera of Colombia.[33] Nyakuma et al. through microstructure and mineralogical analyses revealed particles with a rough texture, surface, and glassy luster.[34] These issues should be clarified to reveal the deformation, damage, and failure mechanism of the shaft coal pocket wall. The effective means to investigate these issues was a three-dimensional physical similarity simulation test, which further revealed the deformation, damage, and failure mechanism of the shaft wall.

Thus, the strain of the shaft coal pocket wall of coal mines and development characteristics of surrounding rock fractures were investigated, using the three-dimensional physical similarity simulation experiment of the shaft coal pocket wall at the transparent material and multiple comprehensive test technology monitoring. The interactions of bulk particles, silo walls, and surrounding rocks were also considered in the above discussions. The "gray box" three-dimensional physical simulation test was performed and the experimental results were in good agreement with the field engineering practice. This investigation has an important practical and scientific significance for the research on the stability of the shaft coal pocket wall.

2. SIMILAR MODEL AND EXPERIMENTAL MATERIAL RATIO

The three-dimensional physical simulation experiment of the shaft coal pocket was carried out on the bench independently developed by Xi'an University of Science and Technology. The shaft coal pocket model of the transparent material was customized and processed to directly observe the flow state of internal loose particles through the profile. Similar materials such as river sand, gypsum, and white powder were used to simulate each rock stratum of the surrounding rocks according to different ratios. Joints among different rock layers were also set in layers with mica sheets.

2.1. Three-Dimensional Similar Material Model of Shaft Coal Pocket. Here, the three-dimensional physical similarity simulation experimental platform of the Xi'an University of Science and Technology was adopted in this experiment, which was 1.6 m long, 1.6 m wide, and 1.3 m high in size. The material model of the transparent bottom coal bunker wall was designed with a ratio of 1:20. A large-scale transparent material similarity simulation test will be used in the experiment. Two model scale plans are proposed here. The shaft wall section is Φ 0.4 m (in diameter) ×1.0 m (in height) with a wall thickness of 3 mm. A transparent material shaft coal pocket wall model was customized with acrylic plexiglass. In the model experiment, the diameter of the body is 40 cm with the height and coal outlet diameters of 130 cm and 8 cm, respectively.

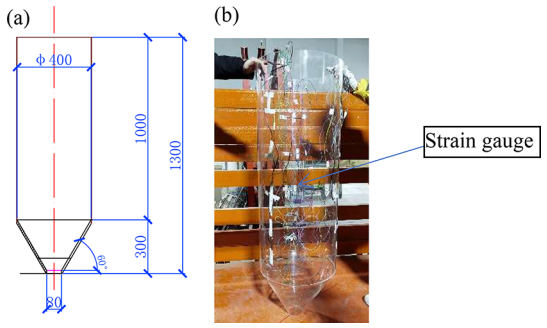

Figure 1. Model and dimension drawing of the transparent shaft coal pocket wall. (a) Borehole peep, and (b) physical model.

Table 1. Physical and Mechanical Parameters of the Transparent Shaft Coal Pocket Wall

density (kg/m^3)	thickness (mm)	breaking strength (MPa)	yield strength (MPa)	elastic modulus (MPa)
1180	3	0.103	0.124	2.758

Table 2. Basic Physical Parameters of Bulk Storage

storage material	density (kg/m^3)	internal friction angle (deg)	internal friction coefficient	external friction coefficient	Poisson's ratio
coal	1000	30	0.38	0.36	0.3
sand	1500	26	0.3	0.32	0.26

The existing 5t lifting and lowering traveling crane device in the laboratory can realize the loading and lifting of bulk particles in the warehouse. A height of 1.0 m shall be reserved at the discharge opening below the wall of the shaft coal pocket to meet the working space. The materials discharged from the bottom shall be cleaned manually. Figure 1 depicts the model size and real transparent shaft coal pocket wall.

2.2. Geometric Similarity Constant. Background: Ganhe coal mine shaft coal pocket is the only one in the mine. It is located at 24.5 m West, north of the main shaft. The actual geometry size for the shaft section of the shaft coal pocket was: diameter Φ = 6.40 m, height h = 27.42 m, and similarity ratio 1:20, according to the actual situation of Ganhe coal mine shaft coal pocket project. The bunker body was damaged for the first time in 2011, and the collapse gradually became serious from the end of 2015 to April 2016. The damaged section is located at a level of +44.8−+62.8 m, with a maximum collapse depth of 5 m, and height of 7−8 m.

The mechanical state, loss characteristics, and stability of the shaft coal pocket were calculated based on the determined geometric similarity ratio, model similarity ratio, and mechanical similarity ratio. The height of the shaft wall used in the experiment was 1.3 m. The diameter and height-diameter ratios of the bottom coal bunker were 0.4 m and 3.2, respectively, belonging to a deep silo.

https://doi.org/10.1021/acsomega.2c00450
ACS Omega 2022, 7, 16442−16453

Table 3. Similar Material Ratio

serial number	rock stratum (from bottom to top)	actual thickness/m	model thickness/cm	cumulative thickness/cm	mixture ratio/river sand:gypsum:big white powder	remarks
1	mudstone	4.3	22	22	8:3:7	
2	coal	0.3	2	24	20:20:1:5	
3	mudstone	5.3	27	50	8:3:7	
4	aluminous mudstone	0.7	4	54	8:4:6	
5	mudstone	5.3	27	80	8:3:7	
6	medium grained sandstone	3	15	95	7:3:7	
7	siltstone	1.1	6	101	7:2:8	
8	fine grained sandstone	1.2	6	107	7:3:7	
9	siltstone	3.5	18	124	7:2:8	

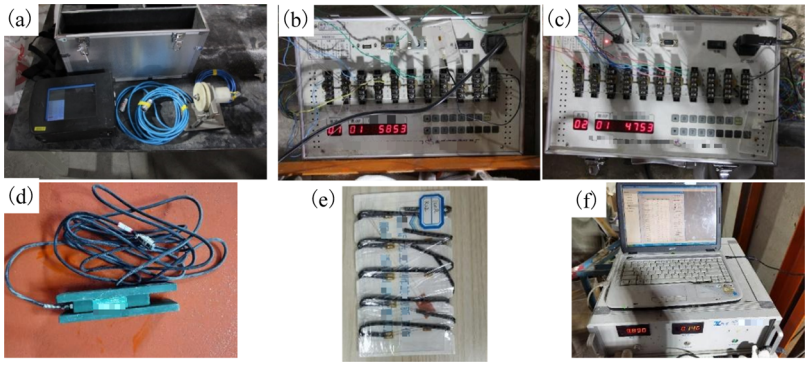

Figure 2. Test instrument. (a) Borehole peep, (b) No. 1 strain gauge, (c) No. 2 strain gauge, (d) pressure sensor, (e)strain gauge, and (f) pressure data acquisition system.

The geometric similarity constant and model design should follow the following similarity conditions

$$C_l = \frac{l_p}{l_m} = 20 \quad (1)$$

Volume−weight similarity constant

$$C_\gamma = \frac{\gamma_p}{\gamma_m} = \frac{1400}{1200} = 1.17 \quad (2)$$

Stress similarity constant

$$C_\sigma = \frac{\sigma_p}{\sigma_m} = C_\gamma \cdot C_l = 23.3 \quad (3)$$

Load similarity constant

$$C_F = \frac{F_p}{F_m} = C_\sigma \cdot C_l^2 = 9333 \quad (4)$$

Time similarity constant

$$C_t = \sqrt{C_l} = 4.47 \quad (5)$$

where the parameter with the subscript "p" represents the prototype value and those with the subscript "m" represents the model value. The l, γ, σ, and F were height, weight, stress, loading, and time, respectively.

2.3. Similar Simulation Materials and Mixture Ratio. The pavement materials of the three-dimensional physical simulation experiment were river sand, gypsum, and white powder, where mica delamination was used for the joint simulation between the rock layers.

2.3.1. **Coal particle simulation material**

For the simulation materials of bulk coal in the bottom coal bunker, the actual rock stratum ratio was adopted with a bulk density of 1.0 t/m^3, which was basically equivalent to the bulk density of coal and gangue stored in the warehouse in the actual production of the mine. The simulated bulk coal material in the warehouse adopts the same material ratio as the above coal seam. Dry sand particles were added as the dispersions with different particle properties, with an unit weight of 1.5 t/m^3. Thus, the test volume of the cylinder and the weight of loose coal particles were $V = \pi R^2 h = \pi \times 0.2^2 \times 1 = 0.125$ m^3 and $G = \rho V = 1000 \times 0.125 = 125$ kg, respectively. The weight of granular sand was $G = \rho V = 1500 \times 0.125 = 187.5$ kg. According to the actual engineering background of the Ganhe coal mine, the experimental material properties are basically the same as the engineering practice, as shown in Tables 1 and 2 for details.

2.3.2. **Similar material ratio**

A similar material ratio of the experimental model and engineering practice was determined based on the geological data of the Ganhe coal mine in Huozhou Mining Area, Shanxi Province, China, which also incorporates with the mechanical parameters of each main rock stratum. Table 3 depicts a similar material ratio of the experimental model and engineering practice.

3. THREE-DIMENSIONAL PHYSICAL SIMULATION EXPERIMENT OF THE TRANSPARENT SHAFT COAL POCKET WALL

3.1. Instruments and Methods. *3.1.1. Instrument.* This physical similarity simulation experiment adopts the multi-means measurement method and also incorporates a comprehensive measurement method in cooperation with the endoscope system. The main measuring instruments used are

https://doi.org/10.1021/acsomega.2c00450
ACS Omega 2022, 7, 16442−16453

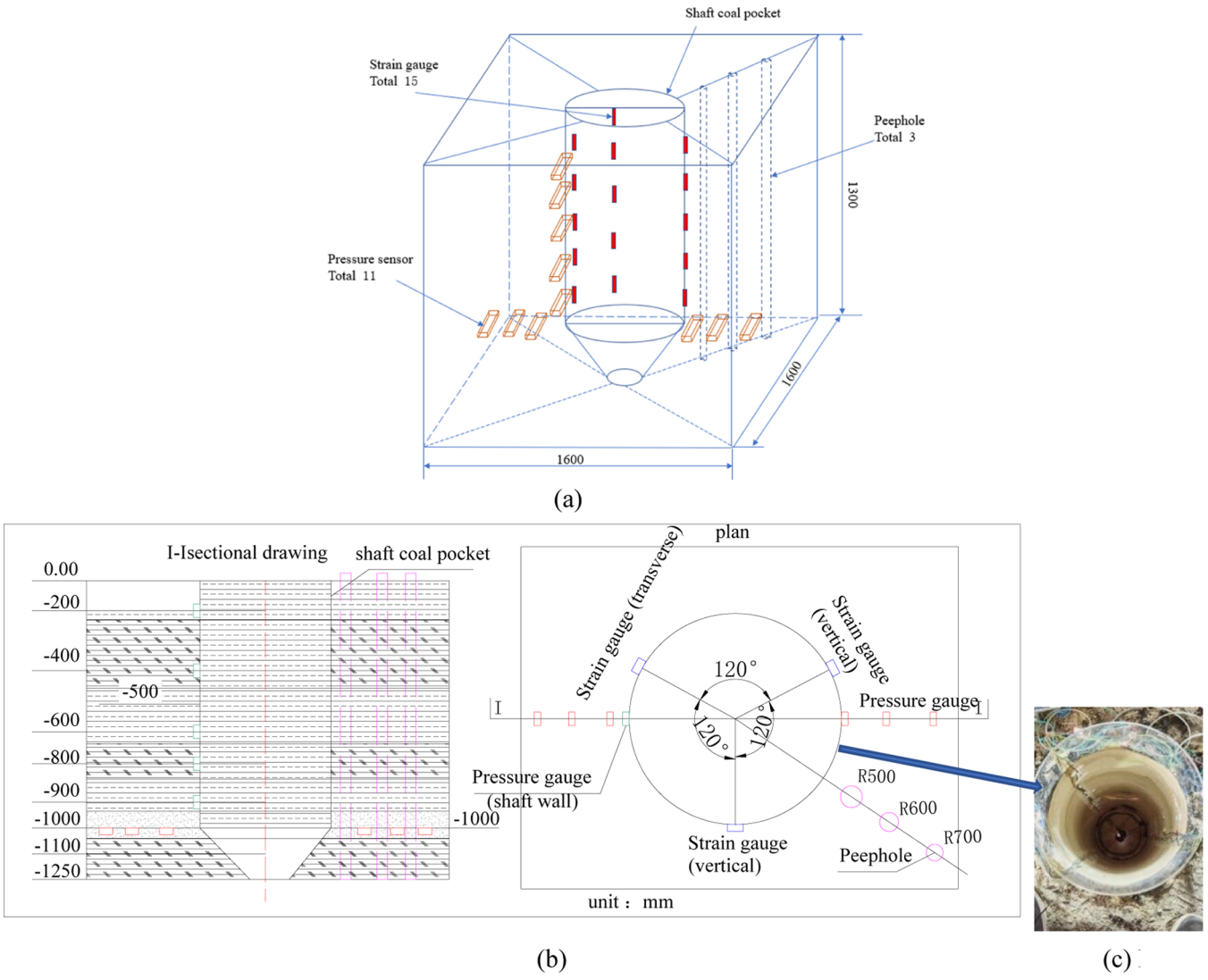

Figure 3. Layout of the strain gauge and pressure sensor in a similar simulation experiment. (a) Three-dimensional schematic diagram, (b) Plan and section, and (c) physical map.

as follows: static strain gauge, pressure data acquisition instrument, borehole peep instrument, computer, and digital camera. The strain gauge and buried pressure sensor were mainly used to measure the circumferential strain and axial strain and the pressure of the shaft wall, respectively, as well as the stress distribution characteristics of the surrounding rock of the shaft. Then, the in situ stress evolution regular pattern in the stratum could be obtained within the simulation range of the shaft coal pocket model. These also include the data of the side pressure of the shaft wall and the surrounding rock stress. Strain gauges and borehole peepers were used to detect the borehole wall strain, displacement, the fracture development, and surrounding rock failure in rock mass, respectively. The overall displacement of particle flow in the bin is measured with a tape measure in the process of coal caving. The whole process of the experiment was captured by a high-definition camera. A CL-YB-114 pressure sensor and the 128 channel sensor data acquisition system were used for the test and analysis. The model of the strain gauge was CM-1L-10. Thus, the deformation of the coal bunker wall and the development of the surrounding rock fissures could be observed by various means at the bottom of the shaft, as shown in Figure 2.

The self-development transparent shaft coal pocket wall was innovatively used for the three-dimensional similarity simulation experiment, whose inside was fulfilled with the simulated materials. The varying cohesion and internal friction angle of different bulk storage particles will exert different lateral pressure on the silo wall. The side pressure loading experiment of the silo wall could be achieved by filling and unloading of the bulk particles. The joints and fissures were preset in advance into the surrounding rocks. A pressure sensor was embedded, as well as the peepholes. The outer side of the silo wall is passively loaded by the surrounding rock constraints. The experiment could be divided into two types: (1) warehouse wall support and (2) without wall support. A total of 40 coal (sand) loading and unloading experiments were carried out in this experiment.

3.1.2. Experimental Test Contents.

(1) Relationship between the side pressure of the shaft coal pocket wall and the bulk storage in the bunker, and the variation of the radial pressure with the height, which were mainly measured by a pressure sensor.

https://doi.org/10.1021/acsomega.2c00450
ACS Omega 2022, 7, 16442−16453

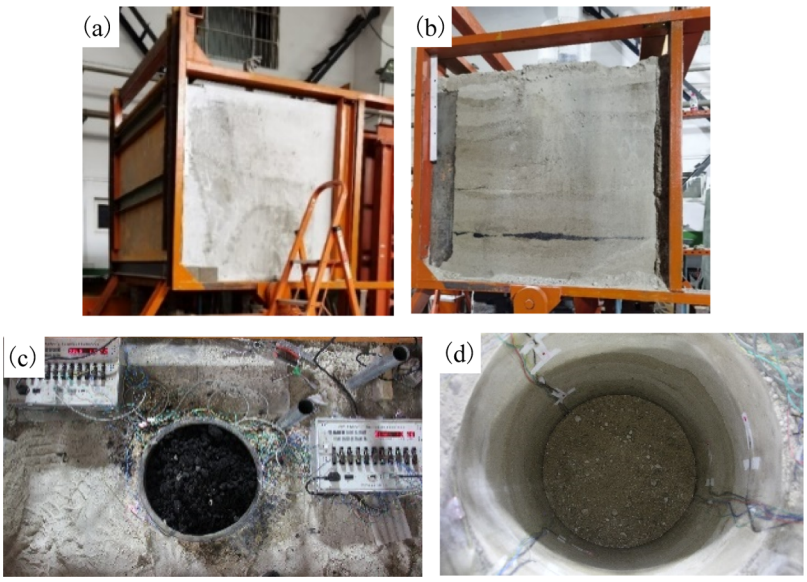

Figure 4. Three-dimensional physical similarity experiment model. (a) Paved physical model (side), (b) physical model (front), (c) top view of the model (coal unloading), and (d) top view of the model (sand unloading).

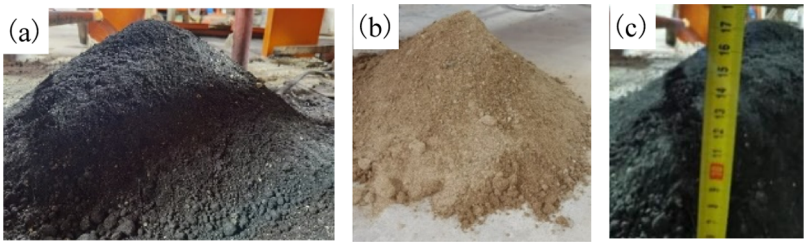

Figure 5. Measurement of the natural angle of repose. (a) Coal particle, (b) sand particle, and (c) height measurement.

(2) Arching situation during the coal (sand) caving process, times of bunker blocking, and arching parameters of the bottom coal bunker in each test.
(3) Influence of different bulk particles on the side pressure of the shaft wall and the relationship between wall deformation and the bulk particles during unloading.
(4) Influence of loading and unloading coal on the surrounding rock cracks considering the existence of support.
(5) Mechanical parameters such as bulk density, internal friction angle, and natural repose angle.

3.2. Experimental Scheme. *3.2.1. Arrangement of Strain Gauge and Pressure Sensor for Simulation Experiment.* The variable angle three-dimensional physical similarity simulation platform, which was self-developed by Xi'an University of Science and Technology was used for the similarity simulation experiment. Multiple comprehensive testing technologies such as the resistance strain gauge test, pressure sensor, and borehole peeping technology were adopted here to explore the variations of the loading, deformation, and loss and to determine the mechanical state, loss characteristics, and stability of the shaft coal pocket. The three-dimensional physical similarity simulation experiment was designed to simulate the shaft coal pocket. Transparent plexiglass was used to design the shaft coal pocket, which could clearly observe the flow of the stored material in the bin. A strain gauge was directly pasted onto the model silo during the experiment. A pressure sensor was directly buried outside of the warehouse wall to detect the side pressure and deformation of the shaft coal pocket wall. The specific arrangements were depicted as follows.

Three measuring points are arranged on the left and right sides of the middle and lower areas of the silo wall cylinder during the experiment. The 15 strain gauges were imbedded into the bill wall and were arranged into three columns (marked as A, B, and C columns). An annular resistance strain gauge was pasted on the outside of the warehouse wall. The 11 pressure sensors were arranged, where 5 of them were buried at the left vertical direction of silo wall to detect the silo wall side pressure. Then, 3 were buried on the left side and 3 on the right side of the surrounding rock outside the warehouse wall. Three peep holes were buried in the surrounding rocks at 500, 600, and 700 mm away from the center of the shaft coal pocket to observe the fracture development of the surrounding rocks. Figure 3 depicts the arrangement of monitoring points, strain gauges, and pressure sensors in the experiment, where Figure 3a–c depicts the three-dimensional schematic of the sensor, layout size, and physical map, respectively.

3.2.2. Similar Simulation Experiment Scheme of Transparent Shaft Coal Pocket Wall. The experiment mainly investigated the interaction relationships among bulk, silo wall, and surrounding rocks via the detection of the borehole wall strain, surrounding rock fracture, and flow pattern of loose particles in different areas of the silo during coal loading and unloading processes in the shaft coal pocket. The three-dimensional box filling was used to simulate the rock stratum.

https://doi.org/10.1021/acsomega.2c00450
ACS Omega 2022, 7, 16442−16453

The relevant stress−strain data, coal level height, and bulk flow pattern shape observation were recorded, as well as the static load and dynamic load overpressure coefficients.

The experimental process can be divided into four stages: (1) sand discharging experiment with the shaft wall, (2) coal caving experiment with the shaft wall, (3) sand discharging experiment without the shaft wall, and (4) coal caving experiment without the shaft wall.

3.3. Three-Dimensional Physical Similarity Simulation Experimental Model. Figure 4 depicts the three-dimensional similarity simulation test model of the shaft coal pocket after paving.

4. RESULTS

4.1. Measurement of Natural Repose Angle of Granular Materials. The bulk particles used in the experiment were similar materials with the same ratio as the simulated coal seam to approach the actual engineering practice. Then, they were crushed into particles as experimental coal bulk particles. River sand and coal particles were, respectively, used as comparative experiments. Figure 5 depicts the measurement of the natural repose angle of loose particles. The natural repose angles of coal particles and dry sand particles were 34.0 and 28.0°, respectively, according to the statistics of 5 groups of natural repose angle data, see Table 4 for more details.

Table 4. Natural Repose Angle Measurement

	natural repose angle (deg)				
test sequence	1	2	3	4	5
coal	33.8	34.1	34.0	34.2	33.9
sand	27.9	28.0	28.1	28.00	27.9

4.2. Side Pressure Distribution of Different Dispersion Particles. The simulation−experiment was conducted considering the existence of the support of bin wall. Figure 6 depicts the variation of side pressure during the second coal caving with the bin wall support. Figure 6a depicts the side pressure curve of the bin wall detected from no. 22, no. 24, and no. 37 sensors during the second coal caving and Figure 6b shows these from no. 22, no. 24, and no. 37 sensors, where the no. 22, no. 24, and no. 37 measures the lower, middle, and the upper areas of the bin wall. From Figure 6, it could be concluded that the side pressure of the silo wall during coal loading is less than that during coal caving for the case of transparent warehouse wall support. The maximum side pressure for the lower detect points during the coal caving could reach up to 310 kPa, significantly higher than the 158.6 kPa of the coal loading process at the same site.

Figure 7 depicts the variations of the shaft wall side pressure curve for the 8th time of sand caving and loading processes. From Figure 7, it could be concluded that the side pressure of the silo wall during sand loading was less than that during sand unloading for the case with the transparent warehouse wall support. The side pressure at the measure point was the largest at the lower part of the shaft coal pocket during the sand unload experiment. For the sand loading process, the maximum value occurred also in the lower area. There is little difference between the coal caving and unloading processes, indicating that sand particles have better fluidity than coal particles. When there is silo wall, there exist a difference in the unloading performance of different bulk particles in the shaft coal pocket. The side pressure of the bulk storage of coal particles was 1.35 times that of dry sand particles. There also exists the maximum silo wall pressure at the middle-lower section during the coal unloading process for the case without a silo wall support, such as the 12th coal loading and unloading processes depicted in Figure 8.

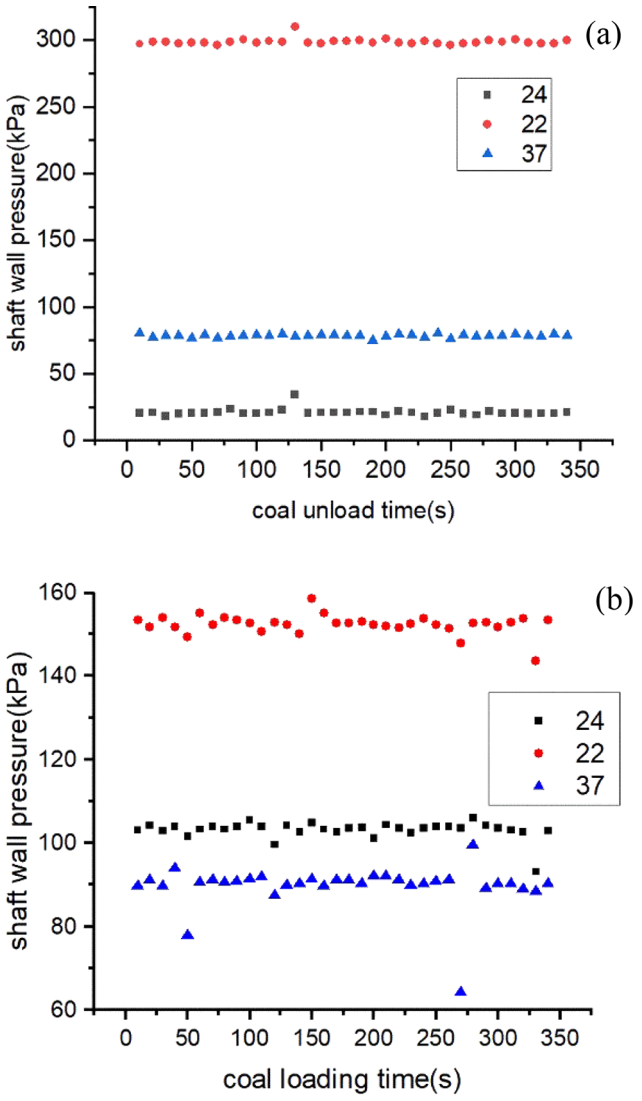

Figure 6. Scatter diagram of side pressure of the bin wall (second time for coal loading and unloading). (a) Second coal caving, and (b) second coal loading.

When there was no transparent warehouse wall support, maximum lateral pressure of the bunker wall during coal loading was close to that during coal unloading (Figure 8), where the maximum pressure also exists at the measuring point at the lower part of the shaft coal pocket for both the loading and unloading processes. In addition, the side pressure of the middle section was significantly higher for the unloading process than for the loading process, indicating the complexity of the effects of the internal mechanical bearing structure of bulk storage in silo during the unloading process. Also, the stress of the silo wall in the middle area is discrete with the strongest fluctuation, which was also the cause for the weak stability of the middle section. Figure 9 depicts the variation of the side pressure during the sand loading process when there was no silo wall support.

https://doi.org/10.1021/acsomega.2c00450
ACS Omega 2022, 7, 16442−16453

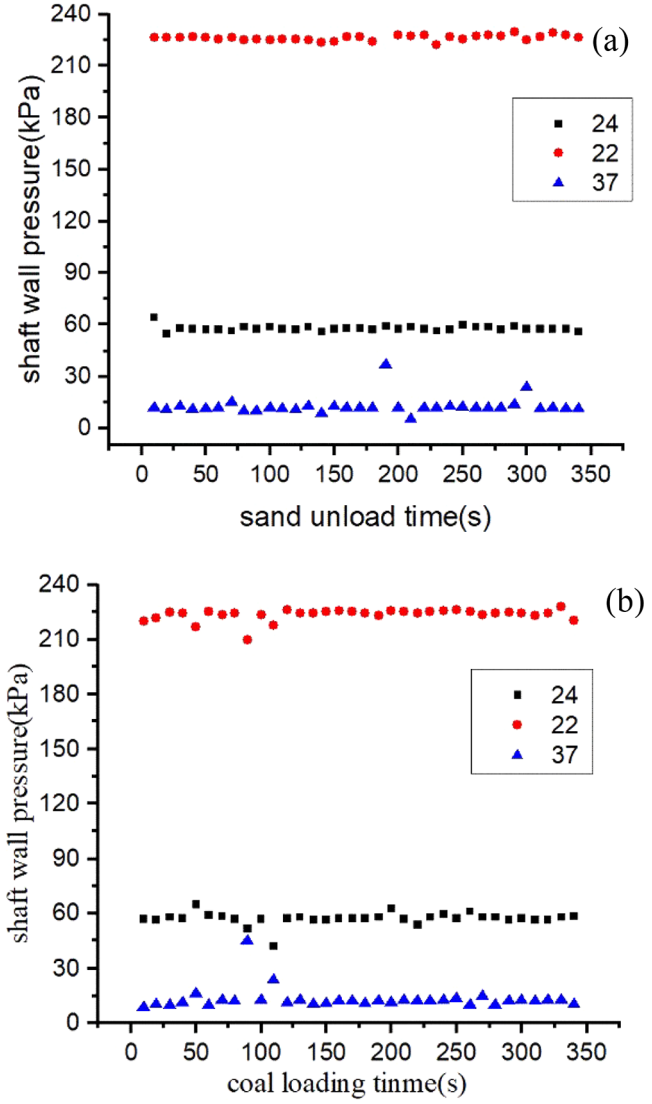

Figure 7. Scatter diagram of side pressure of the shaft wall (8th sand loading and unloading). (a) 8th sand caving, and (b) 8th sand loading.

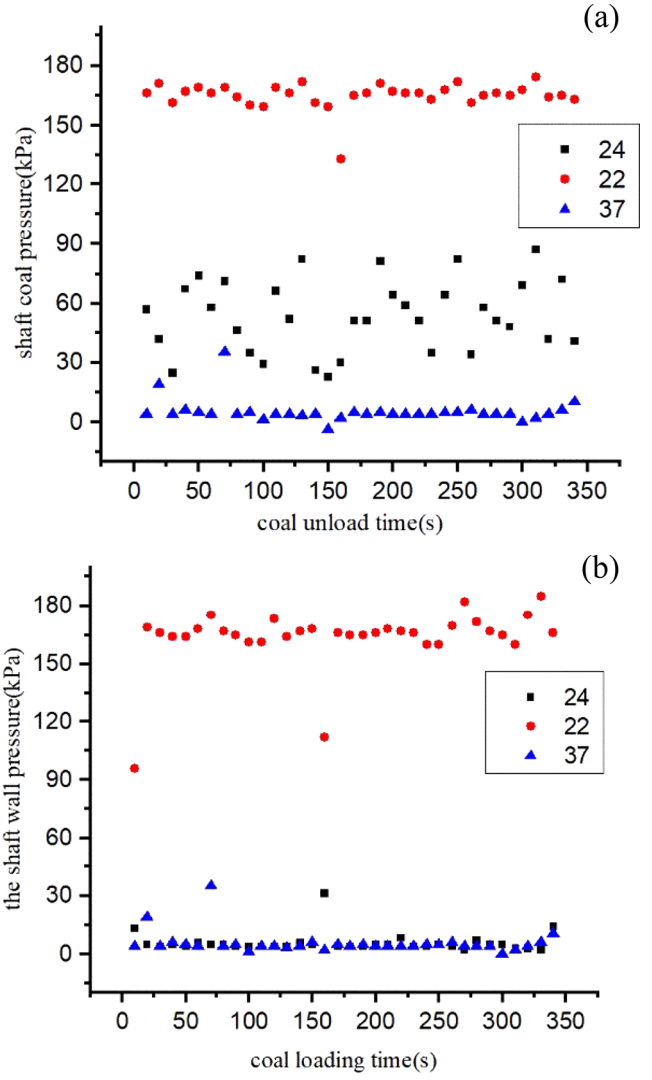

Figure 8. Scatter diagram of side pressure of the surrounding rock (12th coal loading and unloading). (a) 12th coal caving, and (b) 12th coal load.

Similar to the coal loading process, maximum lateral pressure of the bunker wall during sand loading was close to that during sand unloading (Figure 9) when there was no transparent warehouse wall support. The maximum side pressure also occurs at the measuring points of the lower part of the bottom coal bunker for both the sand loading and unloading processes, suggesting the better mobility of the sand particles than the coal particles. The side pressure of the sand particles was significantly higher than the coal particles. From the analysis on the measured data of side pressure of the shaft coal pocket wall, it could be concluded that the middle section has the highest side pressure fluctuation range, followed by the upper section. The lower section has the least side pressure fluctuation range, where all the experiments have indicated that the lower area had the maximum pressure on the inner side of the silo wall.

4.3. Arching Phenomenon during Unloading Process. Coal particles are more likely to form arching than dry sand particles in the unloading process of bulk storage in the warehouse. Also, the arching times of dry sand particles are significantly less than that of coal particles. The blocking times of the coal particles decrease from 8 to 2 compared with dry sand particles at the same bin status when there was silo wall support. When there was no silo wall support, it decreased from 7 to 1. The internal spatial structure was also examined when the arching phenomenon occurs for each experiment. The maximum arching height occurred in the second coal unloading test with a warehouse wall support with a model arch height of 42 cm.

5. DISCUSSION

5.1. Deformation Characteristics of Shaft Coal Pocket Wall. The value of shaft wall strain data about measuring line 2 shown as Table 5.

Figure 10 depicts the silo wall strain of measure line 2 in the vertical direction when there was a transparent warehouse wall support.

From Figure 10, it could be concluded that the maximum strain occurred at −75 cm away from the position of the top surface in the vertical section during the unloading process. This also reflected the high proneness of the stress concentration in this section. The strain in the vertical

https://doi.org/10.1021/acsomega.2c00450
ACS Omega 2022, 7, 16442−16453

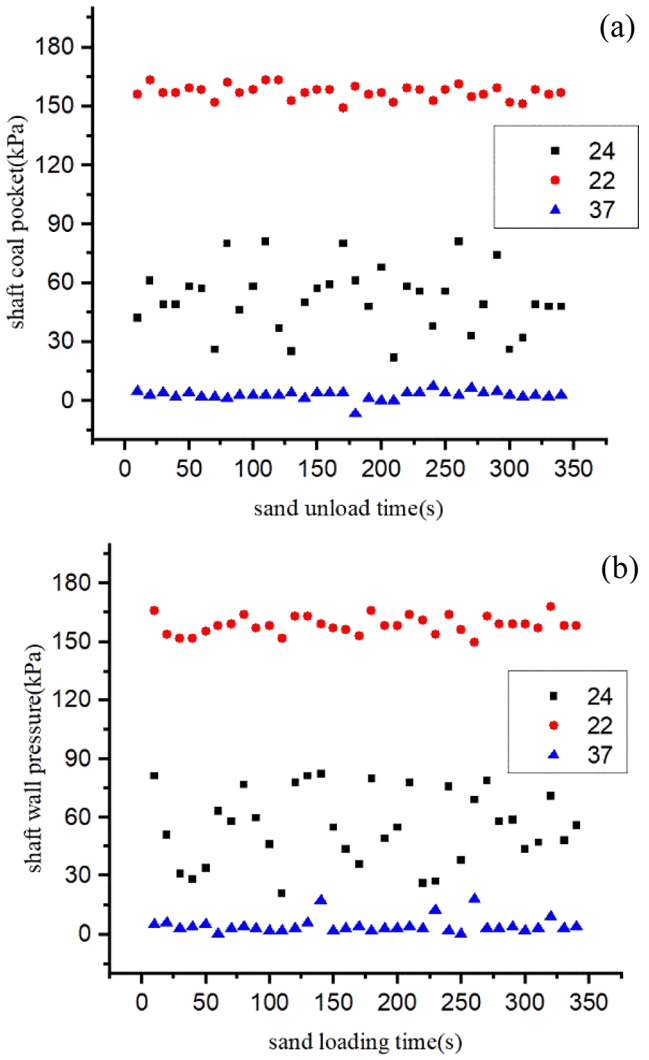

Figure 9. Scatter diagram of side pressure of the bin wall (16th sand loading and unloading). (a) 16th sand caving, and (b) 16th sand loading.

Table 5. Measuring Line 2 Strain Data

depth (cm)	−20	−40	−60	−75	−90
strain (%)	0.6	6	2	22	20

direction is smaller than that in the circumferential direction. Figure 11 depicts the three-dimensional distribution of the silo wall strain obtained via the full data analysis of three survey lines on the shaft coal pocket wall.

The measure points P12 and P22 were used to detect the vertical strain of shaft coal pocket wall in Figure 11. However, the measure points P13, P23, and P33 were used to detect the circumferential strain of the bottom coal bunker wall. The circumferential strain of the shaft coal pocket wall was much greater than the vertical strain, which is mainly due to the large circumferential deformation of the bottom coal bunker wall induced from the extrusion and venting of the bulk storage material in the bunker. However, the vertical direction had the lower deformation extent due to the limited moving space induced from the supporting function of the loading chamber of the lower shaft coal pocket.

5.2. Fracture Development and Loss Characteristics of Shaft Coal Pocket Wall. Figure 12 depicts the fracture

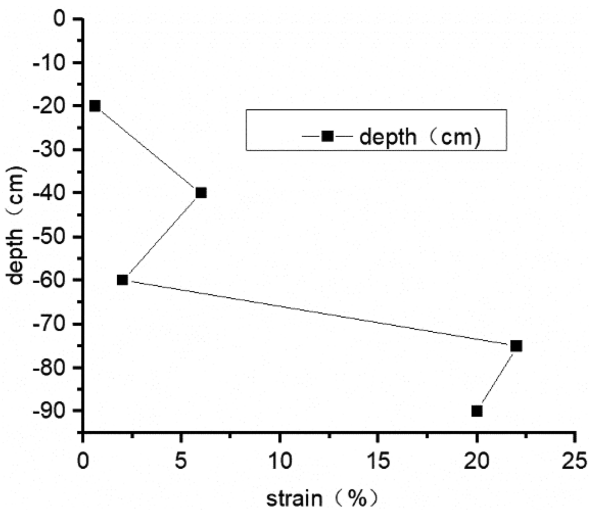

Figure 10. Measured value of shaft wall strain.

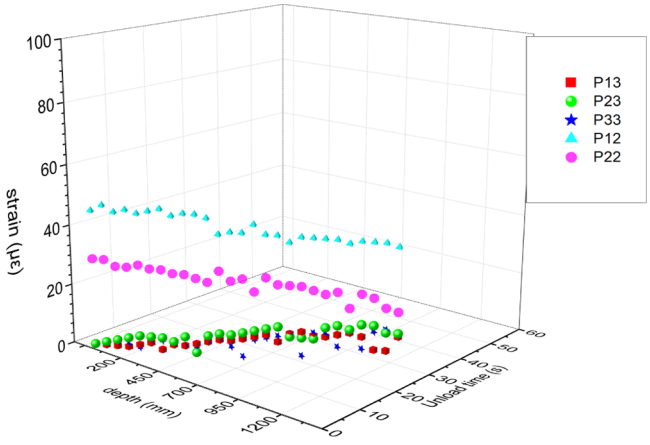

Figure 11. Three-dimensional distribution of the shaft wall strain.

development characteristics of the surrounding rocks of the no. 1 peephole, which was the nearest to the bin wall. There were no fracture development for both the upper (Figure 12a) and middle areas (Figure 12b) of borehole 1 after 40 coal loading and unloading experiments. However, two microfractures were developed in the lower region of the no. 1 peephole (Figure 12c), suggesting that there is a certain disturbance in the surrounding rock with the repeated loading and unloading of coal in the bottom coal bunker. The "weak rock stratum" in the surrounding rocks of the region in Figure 12c played an important role in controlling the deformation and failure of the warehouse wall. It was probable that instability occurs first in this area with the gradual accumulation of the number of stress cycles on the silo wall, which was also the key maintenance area in the actual project.

Figure 13 depicts the fracture development characteristics of the surrounding rocks of the no. 2 peephole. Unlike Figure 12, there were no obvious fracture development for both the upper area (Figure 13a), middle area (Figure 13b), and lower area (Figure 13c) of borehole 1 after 40 coal loading and unloading experiments. This was induced from the fact that the no. 2 peephole was far, up to 20 cm away from the bottom coal bunker wall, and thus the disturbance degree of the repeated loading and unloading was obviously weakened in the bin. Furthermore, the whole process of loading and unloading coal

https://doi.org/10.1021/acsomega.2c00450
ACS Omega 2022, 7, 16442−16453

Figure 12. No. 1 borehole peeper. (a) Surrounding rock in the upper region, (b) surrounding rock in the middle region, and (c) surrounding rock in the lower region.

Figure 13. No. 2 borehole peeper. (a) Surrounding rock in the upper region, (b) surrounding rock in the middle region, and (c) surrounding rock in the lower region.

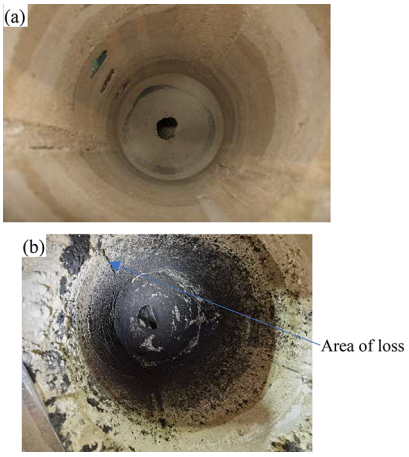

Figure 14. Deterioration of the shaft coal pocket. (a) Intact silo wall before coal unloading, and (b) shaft wall with loss after coal unloading.

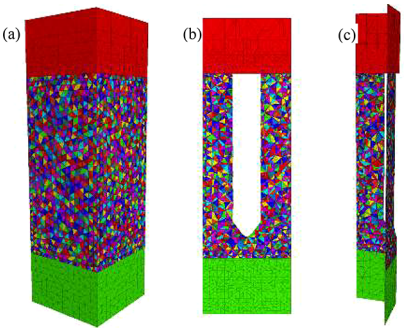

Figure 15. Numerical model. (a) Three dimensional model drawing, b) vertical section, and (c) sector section.

(sand) in the bottom coal bunker had little effect on the surrounding rock disturbance of peephole 3, which was 30 cm away from the bunker wall when the bottom bunker wall was complete.

For the loss characteristics of the shaft coal pocket wall, the shaft coal pocket wall could be gradually damaged by an external force for a long time with increasing coal handling times. Both the elastic modulus of the silo wall and strength of the concrete material could degrade when the coal handling is accumulated to a certain extent. Figure 14 depicts the visible wall loss characteristics during the coal unloading process

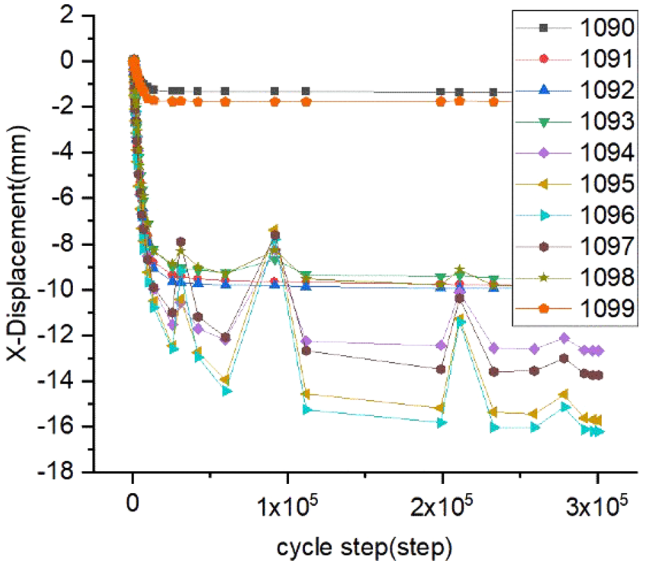

Figure 16. Radial displacement change.

when there was no bin wall. During the unloading process, the loss inside the silo wall occurs with the increase of unloading times and the contact wear between the bulk particles and silo wall materials (Figure 14b).

5.3. Numerical Simulation and Experimental Verification. In order to further analyze the rationality of the experiment, Figure 15 depicts the established numerical model created via 3DEC numerical analysis software.

The stress conditions of the shaft coal pocket wall under the effects of cyclic loading and unloading was simulated via the numerical experiment. The measure points were arranged in the upper, middle, and lower regions of the shaft coal pocket wall to detect the radial displacement of the shaft coal pocket wall. The results are depicted in Figure 16. It can be seen that the radial displacement of measuring point 1095 arranged in the lower area is the largest, while the displacement of measuring point 1099 at the bottom is the smallest. The model size of the numerical experiment was the same as the actual situation. The diameter and wall thickness of the shaft coal pocket were 7 m and 300 mm, respectively. One measuring line was arranged every 5 m. A total of three measuring lines were arranged on the section to monitor the displacement and stress during coal loading and unloading. The specific

https://doi.org/10.1021/acsomega.2c00450
ACS Omega 2022, 7, 16442−16453

Table 6. Parameters of Each Rock Stratum in the Numerical Experiment

rock stratum	thickness (m)	tensile strength (MPa)	compressive strength (MPa)	shear strength (MPa)	bulk density (kN/m^3)	elastic modulus (MPa)	Poisson's ratio	cohesion (MPa)	internal friction angle (deg)
mudstone	4.3	0.80	15.5		24.0	1400	0.32	1.25	31.0
coal	0.3	0.25	17.9		13.3	1300	0.30	1.20	14.8
mudstone	5.3	0.80	15.5		24.0	1400	0.32	1.25	31.0
aluminous mudstone	0.7	0.70	16.2		22.0	1400	0.33	1.10	29.0
mudstone	5.3	0.80	15.5		24.0	1400	0.32	1.25	31.0
medium grained sandstone	3.0	8.10	90.1	18.4	26.6	9890	0.23	2.60	36.0
siltstone	1.1	4.10	42.7	7.2	25.3	7400	0.24	2.80	41.0
fine grained sandstone	1.2	5.40	52.0	9.0	26.5	8600	0.23	3.00	44.9
siltstone	3.5	4.10	42.7	7.2	25.3	7400	0.24	2.80	41.0

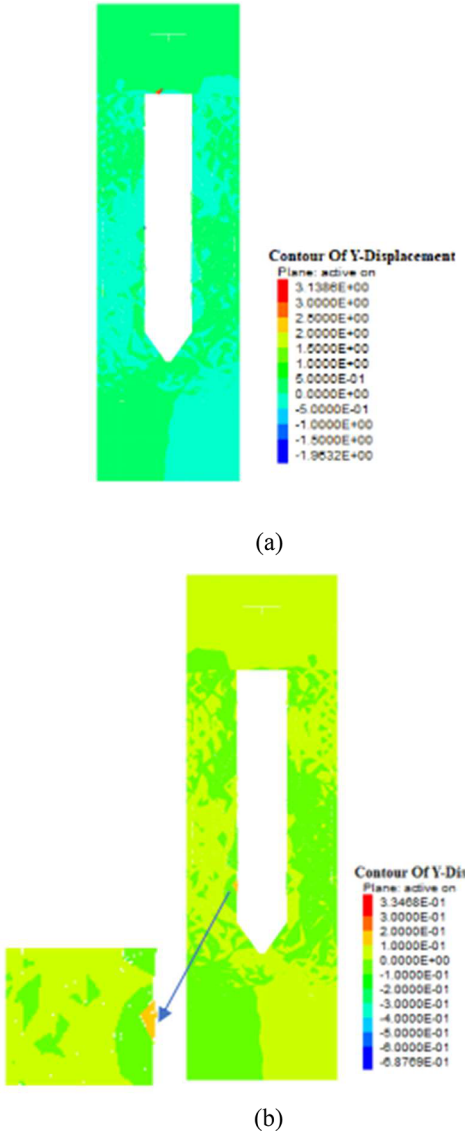

Figure 17. Fracture distribution diagram of numerical simulation test results. (a) 5th cycle and (b) 7th cycle.

parameters of the numerical experiment are shown in Table 6 below.

The numerical simulation results of 3DEC suggested that some units in the middle and lower areas of the silo wall were displaced in both horizontal and vertical directions in the case of internal load change. If the displacement of each unit was not synchronous, fractures appeared first between the two units, suggesting that fractures gradually appeared inside the shaft coal pocket at the bottom of the shaft. The damaged could fall off when the displacement of a unit reached the allowable limit. Then, it would gradually collapse and deteriorate until the warehouse wall if the damaged units further developed. Figure 17 depicts the fracture development. From Figure 17, it could be concluded that the stability of the bin wall at the lower section was worse than in the middle and upper sections of the shaft coal pocket when subjected to cyclic loading and unloading processes. Thus, the lower part was the weak link of project quality control, which needs to be paid close attention. The numerical simulation analysis results were in good agreement with the three-dimensional physical simulation test.

5.4. Stability of Shaft Coal Pocket Wall. The research on the stability of the shaft coal pocket wall needs further development. Experimental research methods also need to transit from two-dimensional to three-dimensional. The experimental results here indicated that the deformation, lateral pressure distribution, and surrounding rock fracture development were the main indexes of the stability of the shaft coal pocket wall. The coal-unloading process of the shaft coal pocket could lead to the changes of stress and displacement of the shaft wall. Unloading overpressure was obvious in the middle and lower parts of the shaft wall. Observing the flow pattern of internal dispersion with the surrounding rocks by using a transparent material shaft wall was a good method, which has not been used in previous studies. The results of the numerical model experiment here can be verified successfully in the coal mine. The investigation of the underground shaft coal pocket wall here could promote the popularization and application of shaft coal pocket technology. Large-scale three-dimensional physical simulation experiment can be closer to the actual project. The lateral pressure distribution regular pattern was also affected by different coal loading forms; however, the coal unloading process was mainly affected by the movement of internal particles, which needs to be further studied in the future.

6. CONCLUSIONS

(1) The three-dimensional physical simulation test was carried out in this paper using the transparent shaft coal pocket wall material to analyze the whole process of

https://doi.org/10.1021/acsomega.2c00450
ACS Omega 2022, 7, 16442−16453

coal loading and unloading. The simulation test of the whole operation process of the shaft coal pocket was investigated using a multi-means comprehensive test system. The flow pattern of the bulk in the shaft coal pocket can be well observed by the transparent cylindrical shaft wall material. The experimental results indicated that the lateral pressure coefficient of the shaft wall in the longitudinal middle and lower areas was larger than that in the middle and upper areas. The measured lateral pressure of the shaft wall can be up to 1.95 times higher than that of dry sand when using coal. The maximum overpressure coefficient measured in the coal unloading process was also greater than that in the sand unloading process. This is in good agreement with the overpressure phenomenon that is more likely to occur in the field engineering when the coal is unloaded from the coal bunker at the bottom of the shaft.

(2) The periodic loading and unloading made the contact force between the loose particles in the shaft coal pocket change significantly. The three-dimensional similarity simulation experiment suggested that using coal as a bulk particle was easier to obtain the arching phenomenon than using dry sand. Also, the arching times of dry sand in the unloading process could be significantly reduced. For the full shaft coal pocket storage with the same drawing height, the times of the silo blocking were 8 times for coal particles and 2 times for dry sand particles on average when there is a shaft wall. However, it was reduced from 7 times to 1 time on average when there is no shaft wall. The unloading overpressure of coal particles was stronger than that of dry sand particles.

(3) Through the three-dimensional physical similarity simulation test, it could also be found that the numerical fluctuation range of the side pressure of the shaft coal pocket wall was the largest in the middle area during the coal loading and unloading processes of the overall structure of the shaft coal pocket, followed by the upper area. The fluctuation of the lower area was the minimum value. The disturbance of the surrounding rock near the warehouse wall was significantly higher than that far away. Some obvious cracks appear in the lower areas of No. 1 peephole 10 cm away from the warehouse wall, which is consistent with the field engineering practice and numerical analysis results.

AUTHOR INFORMATION

Corresponding Author

Mingyin Liu − *School of Energy and Mining Engineering, Xi'an University of Science and Technology, Xi'an 710054, China; Coal Industry Taiyuan Design Research Institute Group Company Limited, Taiyuan 030001, China;* orcid.org/0000-0002-2950-4224; Phone: 86-13233696529; Email: liumingyin2004@163.com

Authors

Yongping Wu − *School of Energy and Mining Engineering and Ministry of Education, Key Laboratory of Western Mine Exploitation and Hazard Prevention, Xi'an University of Science and Technology, Xi'an 710054, China*

Panshi Xie − *School of Energy and Mining Engineering and Ministry of Education, Key Laboratory of Western Mine Exploitation and Hazard Prevention, Xi'an University of Science and Technology, Xi'an 710054, China*

Hongwei Wang − *School of Energy and Mining Engineering and Ministry of Education, Key Laboratory of Western Mine Exploitation and Hazard Prevention, Xi'an University of Science and Technology, Xi'an 710054, China*

Bosheng Hu − *School of Energy and Mining Engineering, Xi'an University of Science and Technology, Xi'an 710054, China*

Complete contact information is available at: https://pubs.acs.org/10.1021/acsomega.2c00450

Notes

The authors declare no competing financial interest.

Data availability: the data used to support the findings of this study are included within the article.

ACKNOWLEDGMENTS

The authors would like to acknowledge the financial supports from the National Natural Science Foundation of PRC (51634007); Major Scientific and Technological Innovation project of the Shandong Province (2019JZZY020326); and Shaanxi Natural Science Basic Research Plan Shaanxi Coal Joint Fund project (2021JLM-10).

REFERENCES

(1) Lv, H.; Ma, Y.; Zhou, S.-c.; Liu, K. Case study on the deterioration and collapse mechanism and curing technique of RC coal bunkers. *Procedia Earth Planet. Sci., Proc. Int. Conf. Min. Sci. Technol.* **2009**, *1*, 606−611.

(2) Yan, H.; Zhang, J. X.; Zhang, S.; Mei, X. C.; Chen, J. L. Macro-micro research on compaction properties of granular backfilling materials. *J. China Coal Soc.* **2017**, *42*, 413−420.

(3) Janssen, H. A. Experiments about pressures of grain in silos. *Z. Ver. Dtsch. Ing.* **1895**, *39*, 1045−1049.

(4) Wu, Y. P.; Hu, B. S.; Wang, H. W.; Xie, P. S.; Liu, M.; Liu, M. Y. Mechanism of flying gangue causing-disasters in longwall mining the steeply dipping seam. *J. China Coal Soc.* **2017**, *42*, 2226−2234.

(5) Wu, Y.; Hu, B.; Lang, D.; Tang, Y. Risk assessment approach for rockfall hazards in steeply dipping coal seams. *Int. J. Rock Mech. Min. Sci.* **2021**, *138*, 104626.

(6) Hu, B.; Wu, Y.; Wang, H.; Tang, Y.; Wang, C. Risk mitigation for rockfall hazards in steeply dipping coal seam: a case study in Xinjiang, northwestern China. *Geomatics, Nat. Hazards Risk* **2021**, *12*, 988−1014.

(7) An, H.; Wang, X.; Fang, X.; Liu, Z.; Liang, C. Wall normal stress characteristics in an experimental coal silo. *Powder Technol.* **2021**, *377*, 657−665.

(8) Baral, S. C.; Daganzo, C.; Hood, M. Optimum bunker size and location in underground coal mine conveyor systems. *Int. J. Min. Geo. Eng.* **1987**, *5*, 391−404.

(9) Yang, H.; Xu, W. J.; Zhang, Q. B. Macro- and meso-mechanism of strain localization in granular material. *Chin. J. Rock Mech. Eng.* **2015**, *34*, 1692−1701.

(10) Wu, Y. P.; Liu, M. Y.; Lv, W. Y.; Hu, B. S. Mechanical model of underground shaft coal pocket and deformation of silo wall in coal mines. *Adv. Civ. Eng.* **2020**, *2020*, 8892091.

(11) Wu, Y. P.; Liu, M. Y.; Xie, P. S.; Lang, D. Three dimensional structure analysis of granular particles in the shaft coal pocket. *J. Xi'an Univ. Sci. Technol.* **2021**, *41*, 592−600.

(12) Yang, S. Q.; Chen, M.; Jing, H.-W.; Chen, K.-F.; Meng, B. A case study on large deformation failure mechanism of deep soft rock roadway in Xin'An coal mine, China. *Eng. Geol.* **2017**, *217*, 89−101.

(13) Kang, Y.; Liu, Q.; Gong, G.; Wang, H. Application of a combined support system to the weak floor reinforcement in deep

https://doi.org/10.1021/acsomega.2c00450
ACS Omega 2022, 7, 16442−16453

underground coal mine. *Int. J. Rock Mech. Min. Sci.* **2014**, *71*, 143−150.
(14) Liang, S.; Elsworth, D.; Li, X.; Fu, X.; Sun, B.; Yao, Q. Key strata characteristics controlling the integrity of deep wells in longwall mining areas. *Int. J. Coal Geol.* **2017**, *172*, 31−42.
(15) Gentzis, T.; Deisman, N.; Chalaturnyk, R. J. A method to predict geomechanical properties and model well stability in horizontal boreholes. *Int. J. Coal Geol.* **2009**, *78*, 149−160.
(16) Xiao, S.; Yang, Q.; Dong, G.; et al. Multi-factor dynamic analysis of the deformation of a coal bunker in a coal preparation plant. *Int. J. Coal Sci. Technol.* **2021**, *8*, 1067−1077.
(17) Xin, H. Q.; Huang, Y. L.; Zhang, W. Q.; et al. Research on deformation and crushing rules and acoustic emission characteristics of gangue bulk under the condition of confined compression. *J. Min. Saf. Eng.* **2020**, *37*, 162−168.
(18) Meng, Q.; Han, L.; Sun, J.; et al. Experimental study on the bolt-cable combined supporting technology for the extraction roadways in weakly cemented strata. *Int. J. Min. Sci. Technol.* **2015**, *25*, 113−119.
(19) Bai, Q. S.; Tu, S. H.; Wang, C. Numerical simulation on top-coal arching mechanism. *J. Min. Saf. Eng.* **2014**, *31*, 208−213.
(20) Shen, B. Coal mine roadway stability in soft rock: a case study. *Rock Mech. Rock Eng.* **2014**, *47*, 2225−2238.
(21) Zhang, J. W.; Wang, J. C.; Wei, W. J.; et al. Effect of face dip angle on the drawing mechanism in longwall top-coal caving mining. *J. China Univ. Min. Technol.* **2018**, *47*, 805−814.
(22) Wang, H. J.; Yin, S. H.; Wu, A. X.; et al. Experimental study of the factors affecting the ore flow mechanism during block caving. *J. China Univ. Min. Technol.* **2010**, *39*, 693−698+715.
(23) Cheng, M.; Fu, X.; Kang, J.; Tian, Z.; Shen, Y. Experimental Study on the Change of the Pore-Fracture Structure in Mining-Disturbed Coal-Series Strata: An Implication for CBM Development in Abandoned Mines. *Energy Fuels* **2021**, *35*, 1208−1218.
(24) Basarir, H.; Sun, Y.; Li, G. Gateway stability analysis by global-local modeling approach. *Int. J. Rock Mech. Min. Sci.* **2019**, *113*, 31−40.
(25) Yin, B.; Kang, T.; Kang, J.; Chen, Y. Experimental and Mechanistic Research on Enhancing the Strength and Deformation Characteristics of Fly-Ash-Cemented Filling Materials Modified by Electrochemical Treatment. *Energy Fuels* **2018**, *32*, 3614−3626.
(26) Zhang, K.; Zhang, D.; Zhang, K.; Cao, Y. Capture of Gas-Phase Arsenic by Ferrospheres Separated from Fly Ashes. *Energy Fuels* **2016**, *30*, 8746−8752.
(27) Yang, Z.; Huang, J.; Wang, Z.; Fang, Y. Unique Advantages of Gasification-Coke Prepared with Low-Rank Coal Blends via Reasonable Granularity Control. *Energy Fuels* **2019**, *33*, 2115−2121.
(28) Nedderman, R. M. Prediction of Stress Distribution in a Two-Dimensional Bunker Using the Fixed Principal Axes Method. *Ind. Eng. Chem. Res.* **1999**, *38*, 596−600.
(29) Léonard, G.; Abatzoglou, N. Stress distribution in lubricated vs unlubricated pharmaceutical powder columns and their container walls during translational and torsional shear testing. *Powder Technol.* **2010**, *203*, 534−547.
(30) Akinyemi, S. A.; Adebayo, O. F.; Nyakuma, B. B.; Adegoke, A. K.; Aturamu, O. A.; OlaOlorun, O. A.; Adetunji, A.; Hower, J. C.; Hood, M. M.; Jauro, A. Petrology, physicochemical and thermal analyses of selected cretaceous coals from the Benue Trough Basin in Nigeria. *Int. J. Coal Sci. Technol.* **2020**, *7*, 26−42.
(31) Hood, M. M.; Eble, C. F.; Hower, J. C.; Dai, S. F. Geochemistry, petrology, and palynology of the Princess No. 3 coal, Greenup County, Kentucky. *Int. J. Coal Sci. Technol.* **2020**, *7*, 633−651.
(32) Yalcin Erik, N.; Ay, F. Use of petrological and organic geochemical data in determining hydrocarbon generation potential of coals: miocene coals of Malatya Basin (Eastern Anatolia-Turkey). *Int. J. Coal Sci. Technol.* **2021**, *8*, 510−533.
(33) Guatame, C.; Rincón, M. Coal petrology analysis and implications in depositional environments from upper Cretaceous to Miocene: a study case in the Eastern Cordillera of Colombia. *Int. J. Coal Sci. Technol.* **2021**, *8*, 869−896.
(34) Nyakuma, B. B.; Jauro, A.; Akinyemi, A. S.; Faizal, M. H.; Nasirudeen, B. M.; Fuad, M. A. H. M.; Oladokun, O. Physicochemical, mineralogy, and thermo-kinetic characterisation of newly discovered Nigerian coals under pyrolysis and combustion conditions. *Int. J. Coal Sci. Technol.* **2021**, *8*, 697−716.

https://doi.org/10.1021/acsomega.2c00450
ACS Omega 2022, 7, 16442−16453